Eur. Phys. J. Spec. Top. (2022) 231:4205–4211
https://doi.org/10.1140/epjs/s11734-022-00577-8

THE EUROPEAN PHYSICAL JOURNAL SPECIAL TOPICS

Regular Article

Optimization of a vibrating MEMS electromagnetic energy harvester using simulations

Ilona Lecerf[1,2], Pierre Moritz[1,2], José Elías Angulo-Cervera[2], Fabrice Mathieu[2], David Bourrier[2], Liviu Nicu[2], Thierry Leïchlé[2,3], Frederico Orlandini-Keller[4], Thibaut Devillers[4], Nora M. Dempsey[4], Guillaume Viau[1], Lise-Marie Lacroix[1,a], and Thomas Blon[1,b]

[1] Université de Toulouse, INSA-CNRS-UPS, LPCNO, 135 Av. Rangueil, 31077 Toulouse, France
[2] Laboratoire d'Analyse et d'Architecture des Systèmes, CNRS, 7 avenue du Colonel Roche, 31077 Toulouse, France
[3] Georgia Tech-CNRS International Research Laboratory, School of Electrical and Computer Engineering, Atlanta, GA, USA
[4] Université Grenoble Alpes, Institut Néel, 38042 Grenoble, France

Received 14 January 2022 / Accepted 9 April 2022 / Published online 4 May 2022
© The Author(s), under exclusive licence to EDP Sciences, Springer-Verlag GmbH Germany, part of Springer Nature 2022

Abstract Nowadays, wireless sensor networks (WSN) are becoming essential in our daily life. However, a major constraint concerns the energy power supply. Indeed, batteries need to be recharged or replaced often which implies a limited lifetime for WSN nodes. One alternative consists in harvesting mechanical energy from surrounding vibrations of the environment. Using finite element simulations, we report here a complete guideline to optimize a MEMS electromagnetic energy harvester consisting of an in-plane vibrating silicon frame supporting an array of micromagnets that faces a static 2D micro-coil. The dimensioning of the magnet array and the specific design of the coil are addressed, considering patterned 50 µm thick NdFeB films with out of plane magnetization. The optimization of the electromechanical coupling which allows to efficiently convert the energy results from a trade-off between the high magnetic flux gradients produced by the micromagnets and the maximum number of turns of the facing coil.

1 Introduction

The expanding market of wireless sensors, also referred as the "Internet of Things" in sectors as diverse as automotive, aerospace or biomedical, requires miniaturized power supplies. Indeed, the limited lifespan of batteries represent a major bottleneck for the widespread use of interconnected sensor nodes. The development of sustainable micro-energy sources for small and portable devices therefore became a very active area of research. Among the different strategies investigated, harvesting mechanical energy from ubiquitous vibration via microelectromechanical systems (MEMS) is highly promising [1]. The vibrating energy harvesters (VEH) all share a common architecture consisting of a mechanical oscillator, a transducer and an electronic circuit to properly condition the output power [2]. The energy transduction can be achieved through piezoelectric, electrostatic or electromagnetic means [2]. Electromagnetic transduction, based on the Lenz–Faraday principle, has been efficiently demonstrated at the centimetric scale with the oscillation of a permanent magnet inside a coil [3]. However, miniaturization using conventional microfabrication processes favours different designs such as the (non)-linear motion of a magnetic plate above a coil. Han et al. have demonstrated the advantage of an in-plane operation mode compared to an out-of-plane one, based on numerical simulations and experimental developments [4]. An in-plane configuration indeed favours stronger electromagnetic (EM) interactions between the coil and the magnet. Considering a vibrating plate with uniaxial displacements along x, the electromotive force (emf) e generated is given by [1]:

$$e = -\frac{d\Phi}{dt} = -\sum_{i}^{N} \frac{d\varphi_i}{dt} = -\sum_{i}^{N} \frac{d\varphi_i}{dx} \cdot \frac{dx}{dt} \qquad (1)$$

where Φ is the total magnetic flux through the coil constituted of N turns, φ_i the magnetic flux through each turn i, and $v(t) = \frac{dx}{dt}$ the relative velocity of magnet and coil. Thus, to optimize the emf and the useful electrical power delivered to an electrical load, one needs to enhance the electromechanical coupling $K = \sum_i^N \frac{d\varphi_i}{dx}$ [5,6]. Up to now, the miniaturization of EM-VEH has suffered from a lack of mature technologies for integrated high performance permanent micromagnets [3,7]. Electrodeposition allows producing thin films and arrays of Co-based materials (CoNiMnP [4], CoPtP [8]) but with limited values of coerciv-

[a] e-mail: lmlacroi@insa-toulouse.fr (corresponding author)
[b] e-mail: tblon@insa-toulouse.fr (corresponding author)

ity and remanence, compared to rare-earth based magnets. High-rate triode sputtering combined with topographic or thermomagnetic patterning has been used to fabricate arrays of NdFeB micromagnets with magnetic properties comparable to the best sintered bulk magnets [9]. The maximum thickness of topographically patterned NdFeB micromagnets has recently been increased to 50 µm [10]. In this framework, several works have recently dealt with the optimization of EM–VEH through magnet design [4,8]. Only a few also take into consideration the complete VEH design, despite the critical role played by the coil design [11,12]. Here we report on a numerical study to optimize the electromechanical coupling of an in-plane operated EM-VEH consisting of an array of perpendicularly magnetized NdFeB micromagnets coupled to a dedicated planar coil. Considering the inherent technological and size constraints for MEMS, general trends are proposed to maximize the magnetic flux gradient by optimizing the magnet array features (size, interspacing) with respect to the coil design. Interestingly, efficient electromechanical coupling thanks to coil design optimisation can be obtained even for thin film like magnets, which are typically considered inappropriate for use in such devices [4,8].

2 Methods

2.1 System

The EM-VEH considered in this study is similar to the in-plane VEH developed by Han et al. [4]. As shown in Fig. 1a, it consists in a 2D rectangular planar coil of N turns facing a vibrating plate connected to a frame by folded beams. The in-plane oscillating motion of the plate is induced by the surrounding ambient mechanical vibrations, typically varying from few Hz to 1 kHz. The vibrating part of the device is designed to have (i) a resonance frequency f_0 in this range, *(ii)* well separated in-plane and out-of-plane resonant modes to avoid any out-of-plane motion, and *(iii)* a limited size as it is for MEMS application. These different criteria lead here to a plate of 6×4 mm^2 with four folded beams, each of them consisting of 3 folds of width 175 µm (Fig. 1a). Considering mechanical robustness and durability, all of these elements are designed out of a 525 µm-thick Si substrate, which leads to an in-plane resonant frequency f_0 = 750 Hz as determined by finite element calculations. To address lower vibrations, the folded beams and the vibration plate dimensions could be adjusted. The magnetic array which covers the 6×4 mm^2 plate consists of NdFeB rectangular cuboids of lateral sizes L and thickness T. The magnet array is not concentric with the overall facing coil, rather it is centred with respect to the turns on one side of the coil. Based on recent advances with thick film fabrication and patterning [10], we considered arrays of micromagnets of thickness T = 50 µm and lateral sizes L varying between 100 µm and 500 µm, with interspacings $\Delta x = \Delta y$ ranging from 30 µm to 150 µm (Fig. 1b), and remanent magnetization values of 1.2 T (M_r = 955 kA/m) [13]. For the sake of comparison, we also considered larger lateral dimensions (L = 900 µm and a single 50 µm thick magnet with in-plane dimensions 6×4 mm, which may be considered as a thin film like magnet). The total area of the magnet array (including the interspaces) is constant, covering the whole 6×4 mm^2 plate. Contrary to the recent report of K. Paul et al. [11] the magnet array's thickness T is kept constant, thus altering the total magnetic volume. Indeed, the magnetic volume depends on the number of magnets within the array, and thus varies as a function of L and Δx.

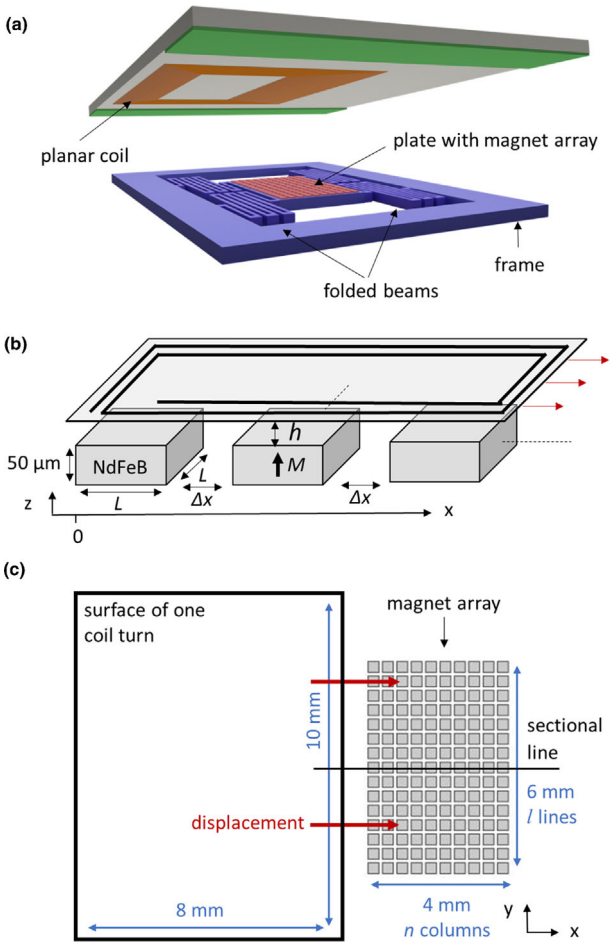

Fig. 1 **a** Design of the vibrating energy harvester considered here. The vibrating plate is connected to the frame by 4 folded beams (each containing 3 folds). The magnetic array is on the 6×4 mm^2 vibrating plate and centred with respect to the turns on one side of the facing planar coil. **b** Schematic view of 50 µm-thick NdFeB cuboids constituting the *(xy)* magnet array with out-of-plane magnetization. Cuboids have a lateral dimension of L and interspacing of Δx, **c** Geometry considered in the simulation: a 10×8 mm^2 surface, representing one coil turn, is displaced above the 6×4 mm^2 magnet array constituted of n columns and l lines

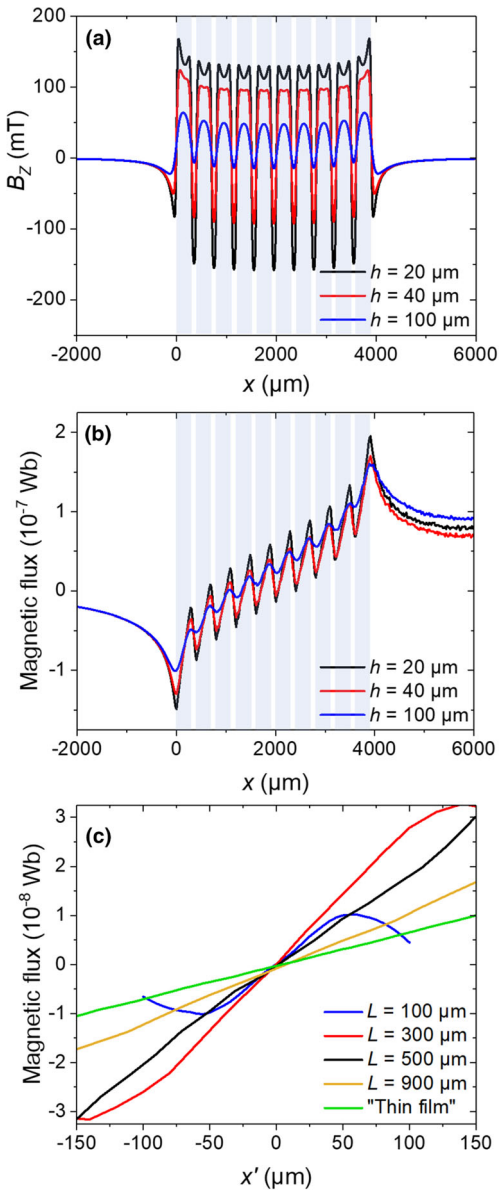

Fig. 2 **a** Profile of the z component of the magnetic induction along the sectional line displayed in Fig. 1 for different magnet-coil distances h for an array of magnets with L = 300 μm and Δx = 100 μm. (Shaded areas correspond to the location of the magnet columns) **b** Magnetic flux through the coil surface as a function of its relative distance from the magnet array: h = 20 μm (black line), h = 40 μm (red line) and h = 100 μm (blue line). **c** Magnetic flux for h = 40 μm above the central column of magnets (indicated by black lines in b) for magnet arrays with different L and Δx = 150 μm. The magnetic flux values have been shifted so as to have $\varphi = 0$ at the centre of the column, corresponding to abscissa $x' = 0$

2.2 Finite element analysis

Considering a perfectly sinusoidal motion with an amplitude A_0 and a frequency f, the velocity becomes $v(t) = dx/dt = A_0\omega \cdot \cos(\omega t)$ with the pulsation $\omega = 2\pi f$, thus:

$$e = -K.v = -\sum_{i}^{N} \frac{d\varphi_i}{dx} \cdot A_0\omega \cdot \cos(\omega t) \qquad (2)$$

One can easily estimate the electromechanical coupling K from the sum of the magnetic flux gradients through the N turns of the coil. Finite element modelling was performed using a simple calculation principle, shown in Fig. 1c. Instead of calculating all of the N magnetic flux gradients, a single surface of 10×8 mm^2 is displaced incrementally along x above the entire 6×4 mm^2 magnet array, the magnetic induction and the resulting magnetic flux are then calculated at each step using the "magnetic field no currents" (mfnc) module of COMSOL MultiPhysics® . The magnetic flux gradients through each of the N turns are then obtained by simply deriving the magnetic flux at each of their specific positions. The studied parameters to be optimized are the lateral size of the magnets L in a magnet array (100, 300, 500, 900 μm), their interspacing Δx (30, 50, 100, 150 μm) and the coil-magnet distance h (20, 40, 100 μm). Contrary to previous studies [4,8,11], the coil-magnet distance h = 10 μm was not considered here as it is expected to be too difficult to implement in a real device. The number n of columns is adjusted as a function of L and Δx so that the magnetic array fits on the 6×4 mm^2 plate.

3 Results

3.1 Magnetic flux gradient

The magnetic flux density and the corresponding magnetic flux created by the n columns ×l lines of magnets (L = 300 μm, Δx = 100 μm, n = 10, l = 15) along the sectional line displayed in Fig. 1c are shown in Fig. 2a, b, respectively, for three different coil-magnet distances h (20, 40, 100 μm). The B_z vertical component of the magnetic induction is the only one considered here as the coil is in the (x,y) plane and the total magnetic flux is given by $\Phi = \int_S \vec{B} \cdot \vec{dS}$.

The magnetic flux density is locally positive and maximum above each column of magnets and negative in between, as a result of magnetic flux closure around each magnet. The magnetic flux varies similarly. When the coil surface is above a magnet column, the magnetic flux gradient $d\varphi/dx$ is positive, while in between the magnet columns, the magnetic flux gradient is negative. The amplitude of the magnetic induction generated by each magnet, and thus the magnetic flux one, depends on its respective position in the array. Indeed, due to the superposition of flux from neighbouring magnets, smaller inductions are observed above the central magnets (5^{th} and 6^{th} columns) compared to the side-edge ones (1^{st} and 10^{th}).

The coil-magnet distance h strongly impacts the magnetic induction. For coil-magnet distance as small as h = 20 μm, local variations of the magnetic induction profile are clearly evidenced above each column, as

a result of inhomogeneous demagnetizing fields [14]. A further increase of the coil-magnet distance smoothens the magnetic profile and drastically affects the extrema values $B_{Zmin}$and B_{Zmax}. For $h = 40$ µm, negative values of magnetic field density are still observed but they disappear for the largest distance $h = 100$ µm. To fully benefit from the magnetic flux gradients, one will thus try to reduce as much as possible the coil-magnet distance. As a trade-off between performance and technological constraints, we detail here the optimization parameters for a coil-magnet distance $h = 40$ µm.

Table 1 presents the magnetic flux gradient $d\varphi/dx$ determined at $h = 40$ µm for each of the 16 different magnet array configurations considered here ($L = 100$, 300, 500, 900 µm, and $\Delta x = 30$, 50, 100, 150 µm). As the gradient value is column dependent because of different neighbouring environments, Table 1 only reports the value obtained above the central magnet columns (for instance above the 5^{th} and 6^{th} columns when $n = 10$). The results show that the magnetic flux gradient increases with the inter-magnet spacing, independently of the magnet size. This effect results from the reduced negative impact of the oppositely oriented stray field produced by neighbouring magnets, favouring large Δx values, 150 µm here. The evolution of the magnetic flux gradient as a function of the lateral size L is however not monotonic. Figure 2c displays the magnetic flux profiles above the central magnet columns for different L with Δx =150 µm. The flux gradient produced at a given height above a magnet is given by its remanent magnetization and its shape, and for the magnet-coil gap considered here (40 µm), the largest magnetic flux gradients are obtained for a 6×4 mm^2 magnet array consisting of 50 µm-thick individual blocks of $L = 300$ µm separated by Δx =150 µm.

3.2 Electromagnetic coupling

We consider now that the coil is constituted of N turns. As the electromotive force is the sum of the magnetic flux gradients through the N turns (Eqs. (1)–(2)), solely positive $d\varphi/dx$ are sought. According to Fig. 2c, the different wire turns of the coil must be located above each magnet column to benefit from positive flux gradient.

At first, we considered the easiest case which consists in having a coil with one turn above each of the n columns of magnets, i.e. $N = n$. Table 1 presents the resulting magnetic flux gradient obtained as $(d\varphi/dx)_{N=n} = \sum_{i=1}^{n} d\varphi_i/dx$. Maxima are no longer found for the largest inter-magnet distance, contrary to what was found for the magnetic flux gradient $d\varphi/dx$. Indeed, due to the superposition of oppositely magnetized stray fields produced by neighbouring magnet columns on a given magnet column, the maxima result from a trade-off between the field profiles of individual magnet columns and the number of columns n, which depends on L and Δx. In this configuration of one coil turn above each magnet column, dense arrays of small magnets are favoured and the electromagnetic coupling leads to a maximum of 4.4 mWb/m for$L = 100$ µm and $\Delta x = 50$ µm.

This simple coil geometry can be further refined when considering the oscillating motion of the plate. Depending on the technological capabilities, one can consider to design above each column of magnets not only one coil turn but several, namely b, turns. The total resulting magnetic flux gradient is then given by:

$$(d\varphi/dx)_{N=b\times n} = \sum_{j=1}^{b}\left(\sum_{i=1}^{n}\left(d\varphi_i/dx\right)_j\right) \tag{3}$$

3.3 Emf calculation

The electromotive force which can be obtained from the different magnetic arrays considered here were determined combining Eqs. (2) and (3) leading to:

$$e\,(t) = -(d\varphi/dx)_{N=b\times n}.A_0\omega.\cos\left(\omega t\right) \tag{4}$$

where the vibration amplitude A_0 is given by the combined effect of the environment and the vibrating system. The largest amplitude will be reached for the resonant frequency, *i.e.* for $f = f_0$. So, to optimize the electrical performance, both the gradient of magnetic flux and the number of coil turns above each magnet column b need to be maximized, considering a given amplitude A_0. Indeed, the electromechanical coupling $(d\varphi/dx)_{N=b\times n}$ can be considered as not totally independent of the magnet to coil velocity as suggested by Eq. (2). Depending on the amplitude A_0, represented as dashed areas on Fig. 3a–c, b coil turns can be positioned above each column of magnets to benefit from the solely positive magnetic flux gradient. Considering a simple geometrical model:

$$b = \frac{L+s-2(A_0+u)}{s+w} \tag{5}$$

where w and s correspond to the coil features (width and spacing, respectively), while u is the leeway to prevent possible misalignment between both parts of the device. As a result, the larger the lateral size L, the higher number of turns b one could fit in. This is clearly shown on Fig. 3a–c for magnet arrays with $L = 100$, 300 and 500 µm, respectively, the number of coil turns b above one magnet column being displayed as vertical bold green lines and increases from 1 to 6 to 16, with increasing value of L. Considering technological constraints, we focus here on coil turns having a wire width $w = 10$ µm, spacing $s = 10$ µm, a vibration amplitude $A_0 = 70$ µm and a leeway $u = 20$ µm.

The amplitude of the electromotive force has been calculated using Eqs. (3)–(4) together with the optimized b values (Eq. (5)) considering $f = f_0 = 750$ Hz, and $h = 40$ µm. For this purpose, the optimized Δx value for each L in this configuration of $b \times n$ turn coils have been determined as a result of a trade-off between stray field superposition and the total magnetic volume:

Table 1 Electromagnetic performance of different magnet array configurations obtained from finite element calculations, considering $\boldsymbol{h}$ **=40** µm

L (µm)	Δx (µm)	$d\varphi/dx$ (mWb/m)	n	$(d\varphi/dx)_{N=n}$ (mWb/m)	$N = b \times n$	Emf (mV)
Magnet lateral size	Inter-magnet distance	Magnetic flux gradient above the central magnet column	Number of columns	Magnetic flux gradient for one coil turn per magnet column	Total number of coil turns	Electromotive force amplitude
100	30	0.10	31	4.19	31	**0.8**
	50	0.14	27	**4.4**	27	0.7
	100	0.21	20	4.24	20	0.6
	150	**0.22**	16	3.66	16	0.5
300	30	0.16	12	2.61	72	4.4
	50	0.21	11	2.73	66	4.6
	100	0.26	10	**2.92**	60	**5.0**
	150	**0.28**	9	2.73	54	4.6
500	30	0.12	7	1.24	112	5.9
	50	0.14	7	**1.42**	112	**6.8**
	100	0.19	6	1.36	96	6.5
	150	**0.20**	6	1.41	96	**6.8**
900	30	0.09	4	0.61	144	5.9
	50	0.09	4	0.61	144	6.9
	100	0.11	4	**0.67**	144	**7.6**
	150	**0.11**	3	0.51	108	5.8

In bold: maxima values of magnetic flux gradients and emf

small Δx imposes low $d\varphi/dx$ due to stray field superposition but allows a higher number of magnets n. For $L >$ 100 µm, the best emf values are consequently obtained for moderate *adhoc* Δx values, typically around 100 µm (Table 1). The emf determined for each magnetic array configuration are plotted in Fig. 3d as a function of amplitude A_0. For $L = 100$ µm, reduced values of Δx allow a dense magnet array, *i.e.* large n, but with only one coil turn per columns of magnet and limited operational amplitude (Fig. 3a) and therefore low emf values (Fig. 3d). For larger L, additional coil turns can fit above each magnet column (Fig. 3b, c), allowing to drastically increase the emf (Fig. 3d). Coils of up to 144 turns can be used to fully benefit from the largest $L =$ 900 µm magnets considered in this study, compared to the 31 turns used for $L = 100$ µm.

Considering the oscillation amplitude A_0, for every magnet configuration, the emf reaches a maximum for a specific A_0 which allows to combine the largest number N of coil turns according to Eq. (5). Interestingly, thanks to a huge number of turns N, Fig. 3d shows that the single thin film like magnet can compensate for low magnetic flux gradient. However, this configuration is never the optimum. For $A_0 > 100$ µm, efficient EM coupling should promote the use of magnets which are as large as possible ($L = 900$ µm, in this study) to benefit from high magnetic volume and coils with numerous N turns. From a practical point of view, A_0 amplitudes in MEMS VEM-EH are however limited to few tens of µm due to the spring design. Therefore, magnets of $L = 300$ µm or $L = 500$ µm should be preferred as they combine large emf with limited magnetic volume (Table 1). Moreover, while the number of coil turns is seen to drastically increase the emf, it also increases the coil resistance, which here scales with N. However, it is important to keep in mind that the electric power effectively harvested in a EM-VEH system requires the internal coil resistance to be as low as possible [6], which constitutes a limitation in achieving high N coils even if technological solutions are proposed [7].

Thus, for larger output powers, one can (i) reduce the distance h between the coil and the magnets, $h = 20$ µm being technologically achievable and (ii) increase the thickness of the sputtered magnetic film. Thicknesses of up to 100 µm can be expected in future and in that case also, the approach developed here of patterned magnets of hundreds of µm associated with optimally designed coils with moderate resistance should be favored.

4 Conclusion

In-plane operated EM-VEH consisting of an array of micro-sized NdFeB perpendicularly magnetized magnets coupled to a dedicated planar coil have been numerically studied using finite element analysis. Electromechanical coupling, which is essential for energy transduction, is subject to a trade-off between maximizing the magnetic flux gradient produced above the array, by increasing the interspacing between magnets, and on the other hand maximizing the number of coil turns, by reducing the interspacing. Therefore, the full

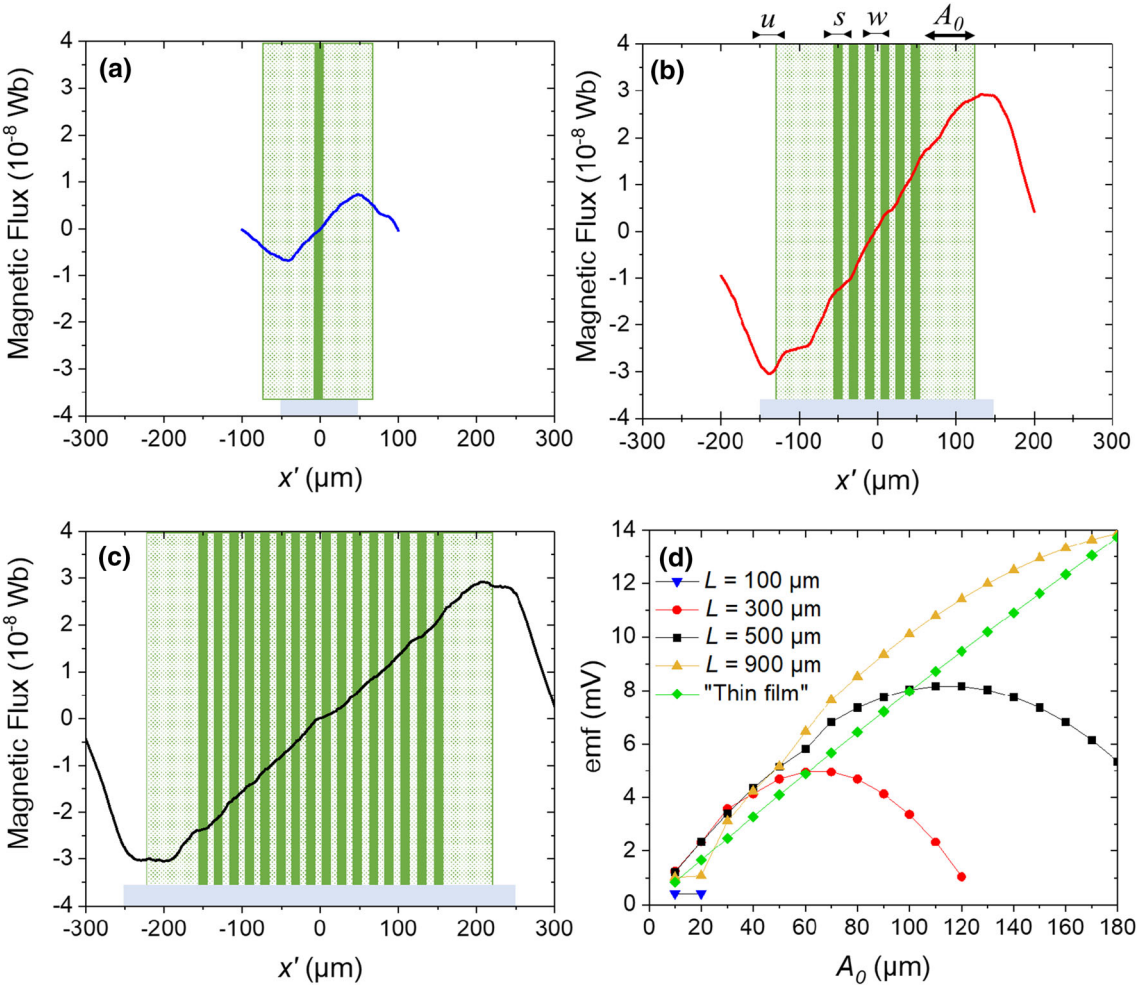

Fig. 3 Magnetic flux along the central column of magnets for the optimized arrays determined by simulation and consisting of **a** $L = 100$ μm, $\Delta x = 50$ μm, **b** $L = 300$ μm, $\Delta x = 100$ μm, **c** $L = 500$ μm, $\Delta x = 50$ μm. The number of coil turns per column b are represented as vertical bold green lines whereas the dashed green area displays the oscillation amplitude. **d** Electromotive force calculated from **a, b** and **c** along with $L = 900$ μm, $\Delta x = 100$ μm, and a single "thin film" like magnet of dimensions 6×4×0.05 mm^3, as a function of the vibration amplitude A_0. The optimized number of coil turns per column of magnet b is optimized for each A_0 using Eq. (5)

optimization of an EM-VEH system requires ad-hoc simulations to fully benefit from the largest potential electromechanical coupling, which depends also on the amplitude of vibration and the distance h between the coil and the magnets. An optimization based only on the stray field profile of the array is clearly not sufficient.

To further improve the performance of the EM-VEH system, the implementation of more complex permanent magnet architectures such as stripes [8,11], bipolar micro-magnet arrays [15] or two magnetic arrays facing each other with opposite magnetization, as recently proposed by Paul et al. [11] is highly promising but requires the specific design of a dedicated coil following the guidelines proposed here.

Acknowledgements This study has been partially supported through the French national project POMADE (ANR 19-CE09-0021-01), the EUR grant NanoX n°ANR-17-EURE-0009 in the framework of the " Programme des Investissements d'Avenir" and the prematuration program of the Région Occitanie (AimCap). PM thanks the Région Occitanie and the Université Fédérale de Toulouse for phD funding.

Data Availability Statement This manuscript has associated data in a data repository. [Authors' comment: The datasets generated during and/or analysed during the current study are available from the corresponding author on reasonable request.]

References

1. *Energy Harvesting Technologies*; Priya, S., Inman, D. J., Eds.; Springer US: Boston, MA, 2009. https://doi.org/10.1007/978-0-387-76464-1
2. C. Wei, X. Jing, A Comprehensive Review on Vibration Energy Harvesting: Modelling and Realization. Renew. Sustain. Energy Rev. **74**, 1–18 (2017). https://doi.org/10.1016/j.rser.2017.01.073
3. Y. Tan, Y. Dong, X. Wang, Review of MEMS electromagnetic vibration energy harvester. J. Microelectromech. Syst. **26**(1), 1–16 (2017). https://doi.org/10.1109/JMEMS.2016.2611677
4. M. Han, Z. Li, X. Sun, H. Zhang, Analysis of an In-Plane Electromagnetic Energy Harvester with Integrated Magnet Array. Sens. Actuators Phys. **219**, 38–46 (2014). https://doi.org/10.1016/j.sna.2014.08.008
5. C.B. Williams, R.B. Yates, Analysis of a micro-electric generator for microsystems. Sens. Actuators Phys. **52**, 8–11 (1996)
6. N.G. Stephen, On Energy Harvesting from Ambient Vibration. J. Sound Vib. **293**(1–2), 409–425 (2006). https://doi.org/10.1016/j.jsv.2005.10.003
7. S. Roy, D. Mallick, K. Paul, MEMS-Based Vibrational Energy Harvesting and Conversion Employing Micro-/Nano-Magnetics. *IEEE Trans. Magn.***2019**, 1–15 https://doi.org/10.1109/TMAG.2019.2896105
8. D. Mallick, K. Paul, T. Maity, S. Roy, Magnetic Performances and Switching Behavior of Co-Rich CoPtP Micro-Magnets for Applications in Magnetic MEMS. J. Appl. Phys. **125**(2), 023902 (2019). https://doi.org/10.1063/1.5063860
9. M. Kustov, P. Laczkowski, D. Hykel, K. Hasselbach, F. Dumas-Bouchiat, D. O'Brien, P. Kauffmann, R. Grechishkin, D. Givord, G. Reyne, O. Cugat, N.M. Dempsey, Magnetic characterization of micropatterned Nd-Fe-B Hard magnetic films using scanning hall probe microscopy. J. Appl. Phys. **108**(6), 063914 (2010). https://doi.org/10.1063/1.3486513
10. F.O. Keller, R. Haettel, T. Devillers, N.M. Dempsey, Batch Fabrication of 50 Lm Thick Anisotropic Nd-Fe-B Micromagnets. *IEEE Trans. Magn.***2021**, 1–1. https://doi.org/10.1109/TMAG.2021.3101911
11. K. Paul, D. Mallick, S. Roy, Performance Improvement of MEMS Electromagnetic Vibration Energy Harvester Using Optimized Patterns of Micromagnet Arrays. IEEE Magn. Lett. **12**, 1–5 (2021). https://doi.org/10.1109/LMAG.2021.3088403
12. P. Wang, K. Tanaka, S. Sugiyama, X. Dai, X. Zhao, J. Liu, A Micro Electromagnetic Low Level Vibration Energy Harvester Based on MEMS Technology. Microsyst. Technol. **15**(6), 941–951 (2009). https://doi.org/10.1007/s00542-009-0827-0
13. R. Fujiwara, T. Devillers, D. Givord, N.M. Dempsey, Characterization of the Magnetic Properties of NdFeB Thick Films Exposed to Elevated Temperatures. AIP Adv. **8**(5), 056225 (2018). https://doi.org/10.1063/1.5007674
14. J.M.D. Coey, *Magnetism and Magnetic Materials* (Cambridge University Press, Cambridge, 2010)
15. K. Yamaguchi, T. Fujita, Y. Tanaka, N. Takehira, K. Sonoda, K. Kanda, K. Maenaka, MEMS Batch Fabrication of the Bipolar Micro Magnet Array for Electromagnetic Vibration Harvester. J. Phys. Conf. Ser. **557**, 012033 (2014). https://doi.org/10.1088/1742-6596/557/1/012033